OPEN ACCESS
IOP Publishing | Songshan Lake Materials Laboratory Materials Futures
Mater. Futures 2 (2023) 025001 (11pp) https://doi.org/10.1088/2752-5724/acbdb4

Polyamorphism mediated by nanoscale incipient concentration wave uncovering hidden amorphous intermediate state with ultrahigh modulus in nanostructured metallic glass

Qiang Luo[1,*], Weiran Cui[2,3], Huaping Zhang[4,5], Liangliang Li[6], Liliang Shao[1], Mingjuan Cai[1], Zhengguo Zhang[1], Lin Xue[1], Jun Shen[7], Yu Gong[2,*], Xiaodong Li[2], Maozi Li[5] and Baolong Shen[1,*]

[1] School of Materials Science and Engineering, Jiangsu Key Laboratory for Advanced Metallic Materials, Southeast University, Nanjing 211189, People's Republic of China
[2] Institute of High Energy Physics, Chinese Academy of Sciences, Beijing 100049, People's Republic of China
[3] University of Chinese Academy of Sciences, Beijing 100049, People's Republic of China
[4] Institute of Physics, Chinese Academy of Sciences, Beijing 100190, People's Republic of China
[5] Department of Physics, Renmin University of China, Beijing 100872, People's Republic of China
[6] Inner Mongolia University of Science & Technology, Baotou 014010, People's Republic of China
[7] College of Mechatronics and Control Engineering, Shenzhen University, Shenzhen 518060, People's Republic of China

E-mail: q.luo@seu.edu.cn, gongyu@ihep.ac.cn and blshen@seu.edu.cn

Received 16 December 2022, revised 9 February 2023
Accepted for publication 21 February 2023
Published 15 March 2023

Abstract

Comprehending the pressure-/temperature-induced structural transition in glasses, as one of the most fascinating issues in material science, is far from being well understood. Here, we report novel polyamorphic transitions in a Cu-based metallic glass (MG) with apparent nanoscale structural heterogeneity relating to proper Y addition. The low-density MG compresses continuously with increasing pressure, and then a compression plateau appears after ∼8.1 GPa, evolving into an intermediate state with an ultrahigh bulk modulus of ∼467 GPa. It then transforms to a high-density MG with significantly decreased structural heterogeneity above ∼14.1 GPa. Three-dimensional atom probe tomography reveals concentration waves of Cu/Zr elements with an average wavelength of ∼5–6 nm, which promote the formation of interconnected ringlike networks composed of Cu-rich and Zr-rich dual-glass domains at nanometer scale. Our experimental and simulation results indicate that steplike polyamorphism may stem from synergic effects of the abnormal compression of the Zr–Zr bond length at the atomic scale and the interplay between the applied pressure and incipient concentration waves

---

[*] Authors to whom any correspondence should be addressed.

2752-5724/23/025001+11$33.00

(Cu and Zr) at several nanometer scales. The present work provides new insights into polyamorphism in glasses and contributes to the development of high-performance amorphous materials by high-pressure nanostructure engineering.

Keywords: metallic glasses, heterogeneity, concentration wave, polyamorphism

The lack of long-range atomic order and the absence of crystalline defects endow metallic glasses (MGs) with a suite of lucrative properties but also make their structure rather challenging to decipher experimentally [1–4]. Even though MGs have relatively structural simplicity without inter- and intramolecular interactions, they are showing increasing complexity and attractiveness in medium-range order (MRO) [5, 6], glass formation [7], relaxation dynamics [8–12], mechanical deformation [13, 14], and energetic rejuvenation [15–17]. Recently, high pressure/temperature investigations have revealed unexpected polyamorphic transitions, including liquid-to-liquid (LTL) and glass-to-glass (GTG) transitions in densely packed MG systems [18–25]. Temperature-induced polyamorphic transitions were observed mostly in supercooled liquids or equilibrium melts [18–20, 26–31]. Results of experiments have shown that LTL transition may be general in MG-forming liquids [10, 11, 18–20, 26–30]. In contrast, pressure-triggered GTG transition was observed only in a few MG systems, most of which are rare earth-based families possessing the exclusive assistance of f-electron delocalization [19–25, 32, 33]. In many other Zr-, Ti-, Fe-, Ni-, Co-, Pb-, and La-based MGs, no such GTG transition was observed [34–40]. However, the two exceptions are a Ca–Al MG and a Pd–Ni–P MG showing abnormal compression behaviors [41, 42], in which s electrons transfer into d orbitals, or some covalent-like bonds change to metallic ones under high pressure. In all the MGs reported showing GTG transition, considerable variation of electronic configurations under compression is necessary [26–42]. This electronic polyamorphism is different from the typical GTG transition in other types of glasses involving obvious change of the directional and open coordination environments [43–46]. At present, atomic cluster packing and reorganization under high pressure are rather elusive in MGs, which hinders the exploration of advanced amorphous metals with outstanding performances under extreme conditions.

Here, we report novel steplike polyamorphic transitions in the $Cu_{46}Zr_{42}Al_7Y_5$ MG with nanoscale concentration fluctuations. With increasing pressure, the low-density MG transforms to a high-density MG through nearly constant-volume reorganizations of local structures in the intermediate-density state, which is strikingly different from the electronic polyamorphism in other MGs showing obvious volume reduction during GTG transition due to electronic-configuration variation. Importantly, the new intermediate-density state shows an ultrahigh bulk modulus of ∼467 GPa. Theoretical simulations reveal significant changes in the pair correlation functions in the first three coordination shells upon compression. At larger length scales, by utilizing aberration-corrected high-resolution transmission electron microscopy (HRTEM), atomic-resolution Z-contrast scanning transmission electron microscopy (STEM), and three-dimensional atom probe (3DAP) tomography, pronounced nanoscale heterogeneity and chemical fluctuations with a wavelength (∼5–6 nm) of incipient concentration waves have been observed. We propose a reorganization scheme of the local ring network, as the structural response motif to pressure, composed of several interconnected Cu-rich and Zr-rich domains at the nanoscale embracing a centered domain, to decipher the novel compression behavior of the current Cu-based MG. The ultrahigh bulk modulus of the intermediate MG state may be associated with supra-nanometer dual-glass structures with different compressibilities and the steplike compression of the Zr–Zr bond length. (Supra-nanometer means that the size of each glass droplet is less than 10 nm, and thus 'supra-nanometer dual glass' is used to distinguish it from the conventional phase-separating MGs). The current findings offer a new perspective on polyamorphism in nanostructured glasses and are of importance for designing advanced MGs by modulating the concentration fluctuations at the nanoscale.

$Cu_{46}Zr_{42}Al_7Y_5$ MG was chosen as the main system of the present study because of its enhanced nanoscale heterogeneity due to Y addition (Y–Zr pair has positive enthalpy mixing) and relative 'simplicity' in terms of not having 4f electrons, nonmetal, or any other special elements with distinct change of electronic structure under pressure. The as-quenched ribbon shows typical amorphous features (figures S1 and S2). However, an abnormal exothermic reaction in the differential scanning calorimetry trace between the glass transition and crystallization events (figure S1) is observed (similar to that of the Pd–Ni–P MG), which indicates a unique local structure of the present alloy showing a possible polyamorphous phase transition in the supercooled liquid [27]. *In situ* synchrotron x-ray diffraction (XRD) patterns during compression and decompression processes for the $Cu_{46}Zr_{42}Al_7Y_5$ MG are shown in figures 1(a) and S3, respectively. The alloy remains in its vitrified state up to 23.0 GPa. The first sharp diffraction peak (FSDP) moves toward larger Q with increasing pressure arising from the compression effect. The FSDP position, Q_1, can be determined accurately by a Voigt line profile fitting, and its evolution with pressure is shown in figure 1(b). The changes of Q_1 with pressure of several other MGs are also included for comparison, including a Ti-based MG without polyamorphism [38] and a Ce-based MG showing typical polyamorphism [32], a newly investigated $Zr_{50.7}Cu_{28}Ni_9Al_{12.3}$ MG (figure S4). With increasing pressure, the Zr-, Ti-, and Ce-based MGs show a continuous increase of Q_1 with decreasing compressibility regardless of whether this MG shows a polyamorphic

Future perspectives

The unique structure of metallic glasses (MGs) with pronounced topological/chemical short-to-medium-range order but no long-range structural order underlies their interesting and excellent properties, which render them attractive for both scientific research and various applications. However, the structure of MGs has been a long-standing mystery, leading to poor understanding of glass formation, deformation, relaxation dynamics, and structure–property relationships. In this work, the observation of a novel steplike polyamorphic transition in an MG with concentration fluctuations is an important contribution toward our fundamental understanding of the heterogeneous structure of MGs under compression. Modulating the chemical/topological heterogeneity at the nanoscale in the future may lead to novel MGs with superb performances and therefore would promote further commercial developments (such as in extreme yet technologically important conditions). A major challenge will be understanding the differences in electronic and structural configurations (at different length scales) that distinguish the different amorphous states of a given MG with polyamorphism. The relationships among glass formation, glass transition, polyamorphism in the glass, and liquid-to-liquid transition in the glass-forming liquid are unresolved issues that offer great opportunities for future study.

transition or not, just as observed in many other MGs [32–40]. In contrast, the as-quenched $Cu_{46}Zr_{42}Al_7Y_5$ MG shows a novel compression behavior, that is, it first undergoes normal compression up to around 8.1 GPa, and then it transforms to an intermediate MG state that is hard to compress. When the pressure is further increased to around 14.1 GPa, the alloy evolves further into a high-density state. Moreover, hysteresis between decompression and compression is observed as a typical feature of polyamorphic transition [21]. The lower right inset of figure 1(b) shows the pressure dependence of Q_1 for another piece of sample, indicating the repeatability of the steplike polyamorphic transitions.

It has been recognized that the FSDP embodies the statistical information of the MRO and average interatomic spacing of a glass [1, 27]. The cubic power law, i.e. $(Q_1/Q_{10})^3 \propto V_0/V_1$ based on the Ehrenfest relation, has been widely used to characterize the density/volume change of MGs [47], where Q_{10} and V_0 are the FSDP position and volume at the initial condition, respectively. (Q_1 and V_1 are values at a given pressure.) Recently, the cluster packing of MGs was found to follow the self-similar rule on a fractal network with a dimension of 2.31, and later a dimensionality crossover at an intermediate length scale was suggested [5]. In particular, from the high pressure investigations of Ce-, La-, Cu-, and Ti-based MGs, it has been found that the density of an MG follows a 5/2 power of the FSDP position [38, 48, 49]. Here, we use both the cubic (3) and fractional noncubic (5/2) laws to estimate the relative volume change. As shown in figure 2(a), the volume of the present Cu-based MG shows an abnormal steplike compression behavior with increasing pressure. In most MGs, the compressibility decreases gradually with increasing pressure, as shown in the inset of figure 2(a) for the Ce-based MG as an example. While in some rare earth-based MGs and a Pd-based MG showing a polyamorphic transition, the compressibility may show a slight increase with pressure after a certain pressure around 1.5–3.0 GPa [42, 50]. This could be associated with f-electron delocalization-induced bond shortening in the former case and change of covalent-like bonds into metallic bonds in the latter. In the present sample, we also found that the compressibility between 2 and 7 GPa is larger than that between 0 and 2 GPa [42, 50]. The key points we stress here are the steplike behavior and the intermediate glassy state with the smallest compressibility in a wide pressure range of ~4 GPa. To illustrate this, we depict the bulk modulus, derived from $K = -V(dP/dV)$, as a function of pressure for the Cu- and Ce-based MGs in figure 2(b). Linear fitting of every five adjacent data was used to obtain the slope (dP/dV) of the center point. The Ce-based MG shows a continuous increase in bulk modulus with increasing pressure with three distinct change rates, which is according to the hierarchical densification behavior [32]. In contrast, the $Cu_{46}Zr_{42}Al_7Y_5$ MG shows an abnormal

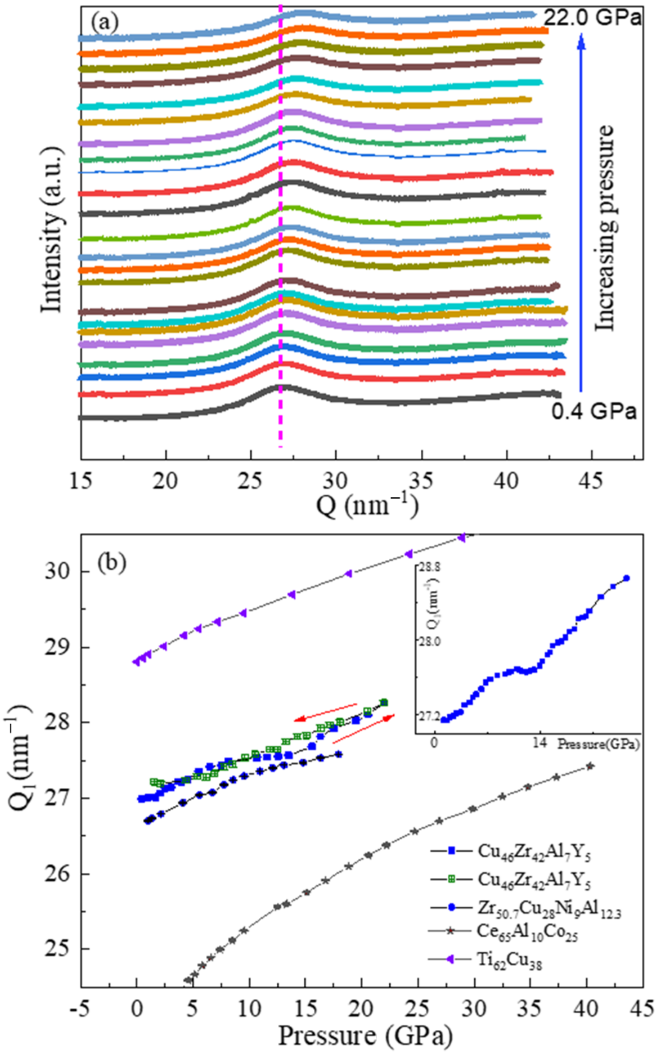

Figure 1. (a) *In situ* XRD patterns of the $Cu_{46}Zr_{42}Al_7Y_5$ MG under different pressures (the arrow shows the detection of increasing pressure). (b) Pressure dependence of Q_1 of $Cu_{46}Zr_{42}Al_7Y_5$ and other MGs for comparison. The solid symbols are for compression, and the open symbols are for decompression; the inset is another independent result of the $Cu_{46}Zr_{42}Al_7Y_5$ ribbon. Error bars are included, and some are smaller than the symbol size.

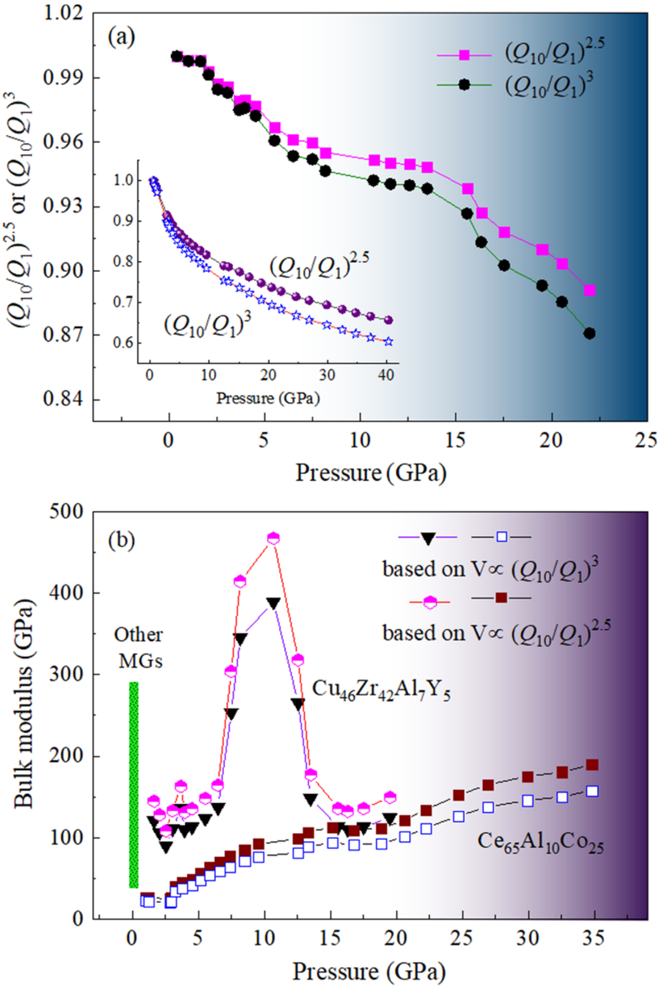

Figure 2. (a) Pressure dependence of $(Q_{10}/Q_1)^3$ and $(Q_{10}/Q_1)^{2.5}$ of the $Cu_{46}Zr_{42}Al_7Y_5$ and $Ce_{65}Al_{10}Co_{25}$ MGs. (b) Pressure dependence of the local bulk modulus of the $Cu_{46}Zr_{42}Al_7Y_5$ and $Ce_{65}Al_{10}Co_{25}$ MGs.

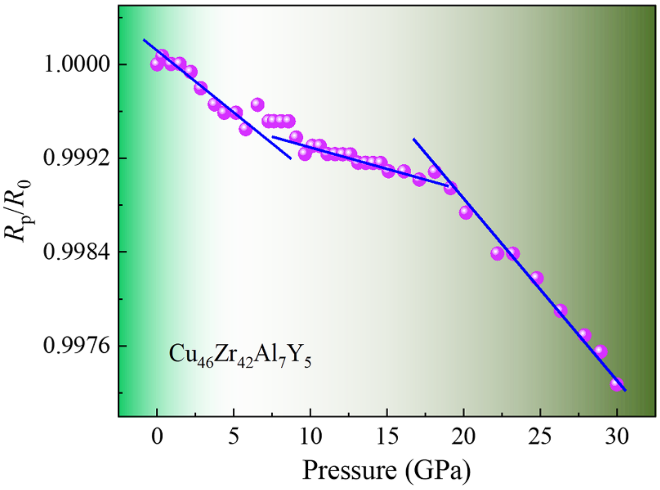

Figure 3. Relative resistivity of the $Cu_{46}Zr_{42}Al_7Y_5$ MG as a function of pressure.

sharp peak between 8.1 and 14.1 GPa, which is consistent with the trend revealed in figure 1(b). In the intermediate state, the bulk modulus can reach up to 467 GPa (using the 5/2 power law), which is much larger than those of typical MGs in the as-quenched state (the marked green pillar in figure 2(b)) [2, 25].

To further verify the abnormal polyamorphic transitions, an *in situ* electrical resistivity measurement under different pressures was carried out. Figure 3 displays a change of relative resistivity with pressure, where R_p and R_0 are the resistivity under high pressure P and ambient pressure, respectively. The resistivity decreases with increasing pressure in the whole investigated pressure range, that is, a negative pressure coefficient of resistivity is obtained. Similar to the volume evolution, the relative resistivity also shows a steplike behavior, and the intermediate MG has the smallest absolute negative pressure coefficient. Since the present Cu-based MG contains no magnetic elements and the experiments were carried out at room temperature, there is no contribution from the effects of Kondo-type s–d exchange scattering, f delocalization, and two-level configurational tunneling. The electrical resistivity mainly arises from disordered atomic scattering described by the structure factor in the framework of the generalized Ziman theory [51] and is thus sensitive to the local structures. Note that the transition pressures of electrical resistivity are similar to those of the FSDP in the XRD patterns. Thus, the abnormal variation of resistivity mainly originates from the complicated three-stage transitions of the local structures of the Cu-based MG. However, at present, the pressure dependence of resistivity of the MG is impossible to illustrate precisely from the detailed change of electronic configuration due to the delicate influence of the Fermi energy E_F, the electron–ion interaction, and structure factor.

To determine the coordinated role of short-range order and MRO on the polyamorphic transition, a combination of *ab initio* molecular dynamics (AIMD) simulations, HRTEM, and 3DAP experiments was performed. Since the AIMD simulations use a box size of ~1.7 nm, the structures at medium-range length scales up to ~2 nm and above cannot be well determined (e.g. from the peak position Q_1 of the static structure factor $S(Q)$). Thus, we focus on the structural changes on short-range scales. Typical atomic configurations from the simulation and the change of potential energy with the atomic volume upon compression are shown in figure S5. Figures 4(a)–(d) show the total and partial pair correlation functions at different pressures. It is observed that the pair correlation functions in the first three coordination shells undergo significant changes upon compression. (The bond angle distribution functions show a slight change, as indicated in figure S6.) In particular, in the first coordination shell, while the peak height in the average pair correlation function $g(r)$ gets enhanced upon compression, the peak height in Zr–Zr partial pair correlation function $g_{Zr-Zr}(r)$ gets suppressed (figures 4(a) and (b)). Importantly, there seems to be a shoulder ahead of the first peak in Zr–Zr partial pair correlation function $g_{Zr-Zr}(r)$ (figure 4(b)). These results indicate that the structural changes around Zr and Cu elements upon compression are very different. In addition, it is found that the first peak position r_1 of $g_{Zr-Zr}(r)$ in the AIMD simulations

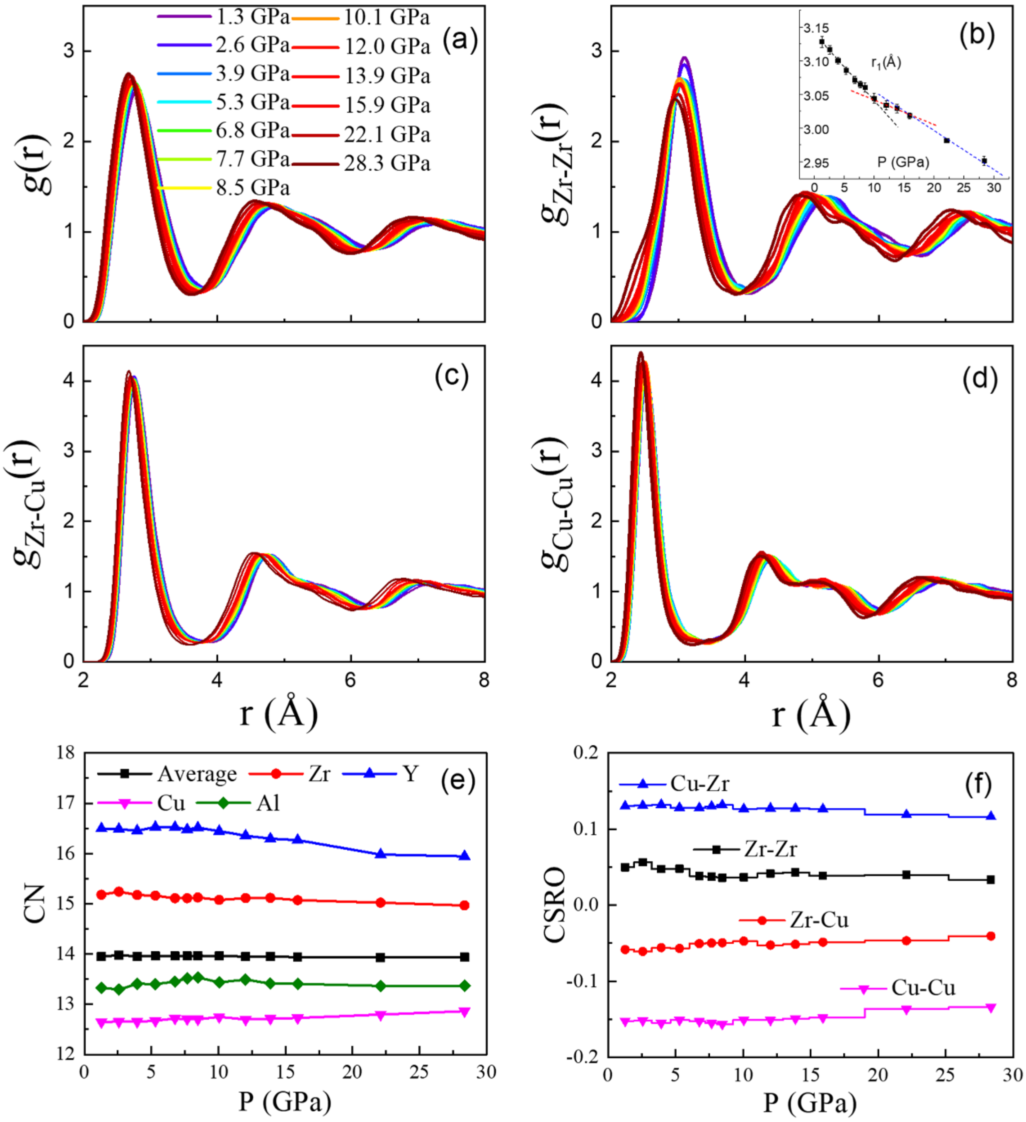

Figure 4. The change of total and partial pair correlation functions with external pressures for the $Cu_{46}Zr_{42}Al_7Y_5$ MG at 300 K, (a) for average pair correlation function $g(r)$, (b) for Zr–Zr pair correlation function $g_{Zr–Zr}(r)$, (c) for Zr–Cu pair correlation function $g_{Zr–Cu}(r)$, and (d) for Cu–Cu pair correlation function $g_{Cu–Cu}(r)$. The inset in (b) is the change of the first peak position of $g_{Zr–Zr}(r)$ with pressure. (e) The change of coordination numbers and (f) chemical short-range orders (CSROs) with external pressures for the $Cu_{46}Zr_{42}Al_7Y_5$ MG.

shows a steplike evolution with the lowest compressibility in the intermediate state (the inset of figure 4(b)), similar to the FSDP of the XRD patterns.

Figure 4(e) shows the change of coordination numbers (CNs) of each element at different pressures. Obviously, the CNs of Al and Cu atoms are smaller than the average CN, whereas the CNs of Zr and Y are larger than the average CN. Upon compression, the average CN stays almost unchanged, while the CNs of Al and Cu atoms increase subtly, and the CNs of Zr and Y atoms decrease. It seems that the CNs of all elements tend to the average CN with increasing pressure. We then calculated the CSROs as

$$C_{\alpha\beta} = 1 - N_{\alpha\beta}/(x_\beta N_\alpha), \tag{1}$$

where N_α is the CN of α element, $N_{\alpha\beta}$ is the partial CN describing the number of β atoms around α element, and x_β is the content of β element. While a negative (positive) value of $C_{\alpha\beta}$ means that there are more (less) β atoms around α element than expected, a zero value means there is no chemical segregation within the first coordination shell. As shown in figure 4(f), $C_{Cu–Zr}$ is negative, and $C_{Cu–Cu}$ is positive, suggesting that Cu atoms prefer to bond with Zr atoms. Whereas $C_{Zr–Zr}$ is negative, $C_{Zr–Cu}$ is positive, indicating that Zr atoms also prefer to bond with Zr atoms. The negative value of $C_{Zr–Zr}$ implies that possible Zr segregation may occur in this alloy. Importantly, both $C_{Cu–Zr}$ and $C_{Zr–Zr}$ shift slightly toward zero with increasing pressure. This suggests that pressure may help to suppress chemical ordering at short-range scales, promoting uniform mixing and eliminating chemical segregation.

We then turn to MRO structures with length scales above 1 nm to further understand the steplike polyamorphic transitions. First, a careful analysis of the HRTEM images was performed to see whether there is contribution from some very

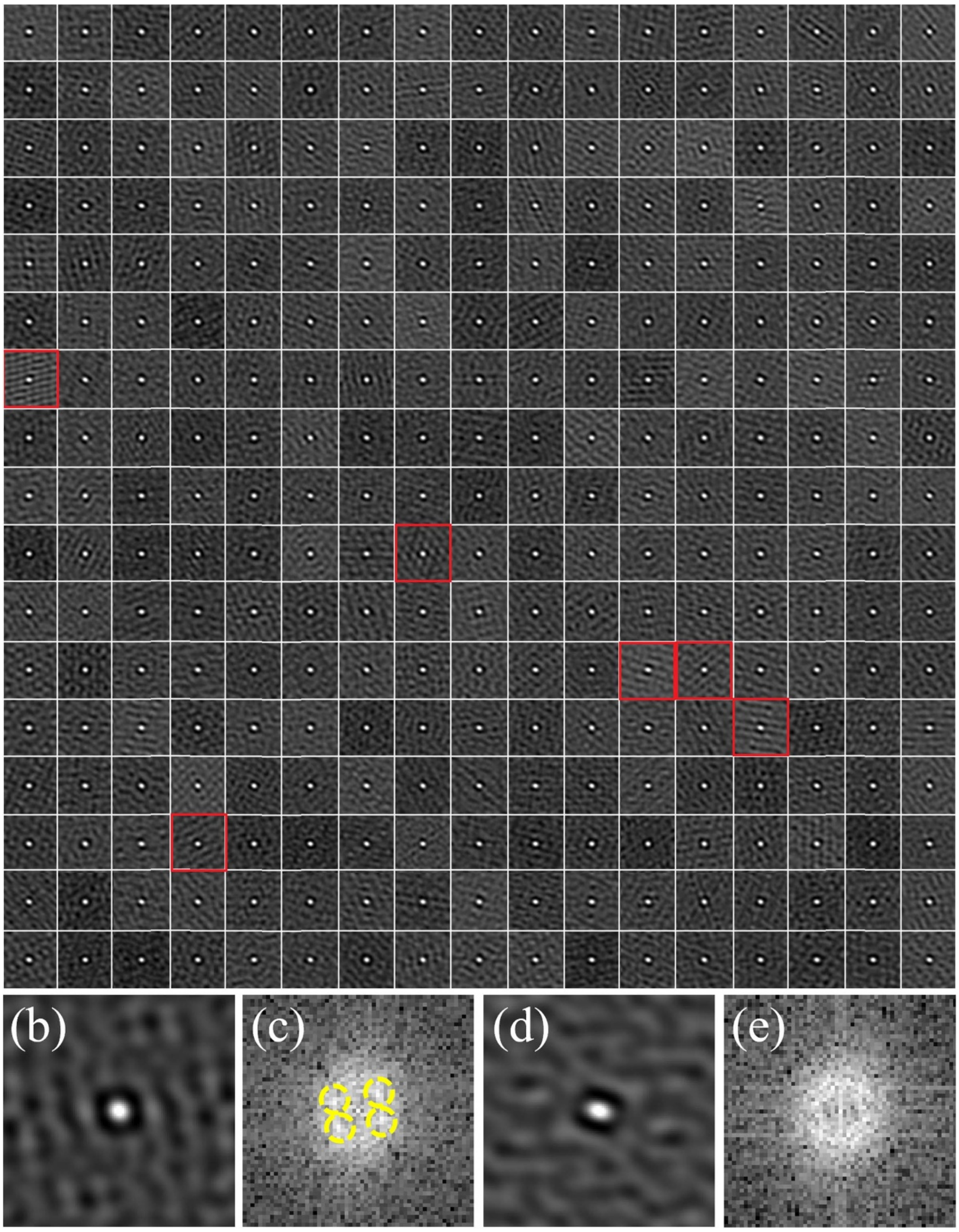

Figure 5. (a) Segmentation of the selected areas in the HRTEM image of figure S2 for autocorrelation analysis of the MG sample. The dimension of each segment or cell is 1.995 × 1.995 nm^2. (b) and (d) are the typical cells with crystal-like order and disordered features, respectively; (c) and (e) are the FFT patterns of (b) and (d), respectively.

fine nanocrystalline clusters or phase separation. Two HRTEM images (one of them is shown in figure S2) were divided into 17 × 17 cells with a size of 1.995 nm × 1.995 nm, and then the image in each cell was transformed into a 2D autocorrelation map to check the local order (figures 5(a) and S7). From the 2D autocorrelation map, a few cells with crystal-like order can be observed (figures 5(b) and (c)), which are marked by red squares in figure 5(a). Figure 5(d) is a typical cell with a totally disordered structure, and its fast Fourier transformation (FFT) pattern is shown in figure 5(e). The area fraction of the crystal-like order regions can be estimated to be ∼2% in the sample. The fraction of the crystal-like regions is lower than that of a $Cu_{46}Zr_{45}Al_7Y_2$ glassy rod of 3 mm diameter [52] due to the better glass-forming ability of the present MG and the larger cooling rate used here to fabricate the ribbon. Therefore, abnormal polyamorphic transitions do not derive from some fine nanocrystalline phases or some special clusters with crystal-like order identified by the presented method.

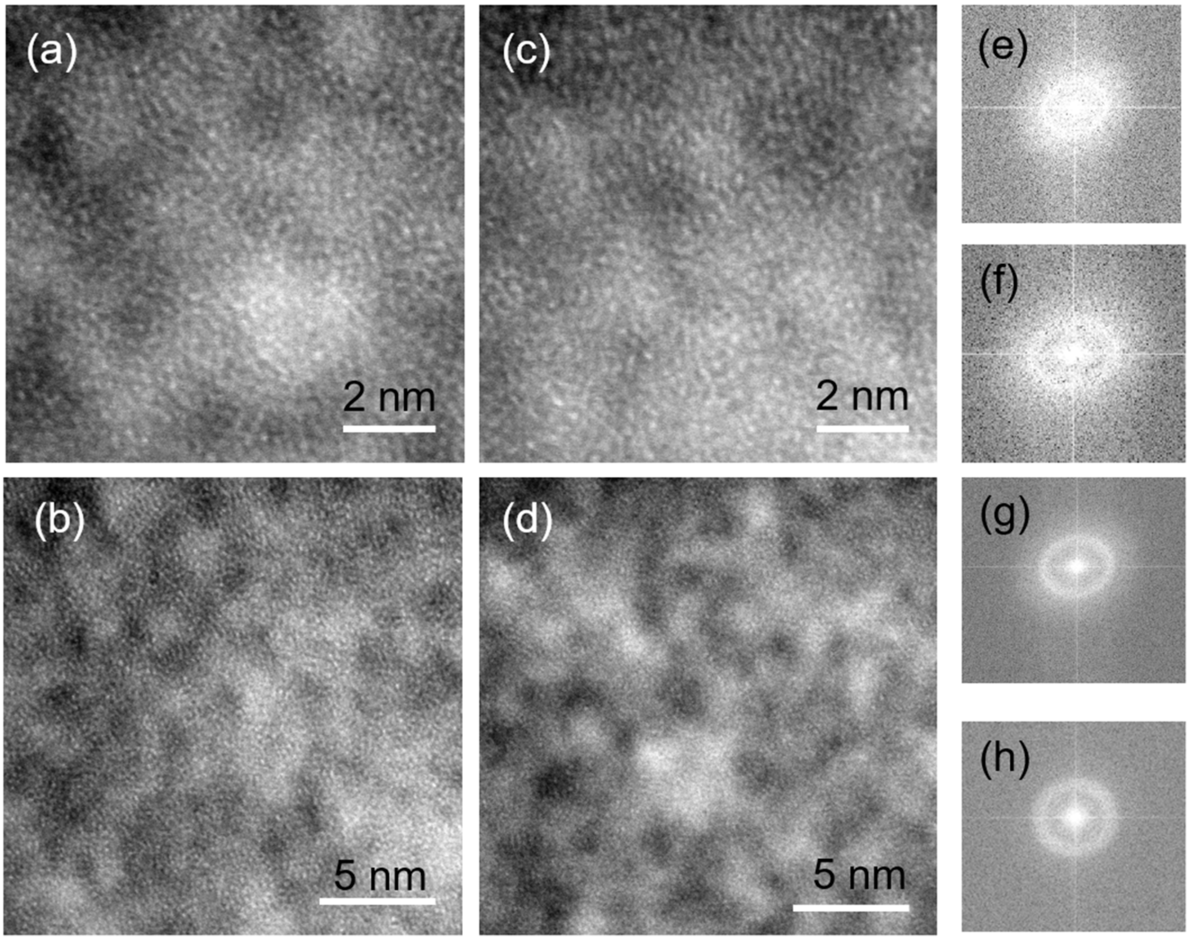

Figure 6. (a)–(d) HAADF-STEM images of the as-quenched $Cu_{46}Zr_{42}Al_7Y_5$ MG. (e)–(h) FFT patterns of (a)–(d), respectively.

Next, we check whether there exist nanoscale chemical or density fluctuations in the present MG, which are not easy to detect by HRTEM. The aberration-corrected high-angle annular dark field (HAADF)-STEM technique with Z-contrast was thus performed, which shows a strong contrast correlated with the atomic number Z of the detecting area. The atomic-resolution HAADF-STEM images in figures 6(a)–(d) show clearly heterogeneous contrast with dark (soft) and bright (hard) domains at the nanometer scale, indicating an inhomogeneous distribution of density and/or chemistry in the present MG. It has been generally accepted that an MG is structurally heterogeneous, which has been revealed from the distribution of modulus, density, and local symmetry [53–55]. By combining angstrom-beam electron diffraction with simulation, the dark and bright domains observed in the HAADF-STEM images of a Zr–Cu–Al MG were revealed to arise from the clusters with crystal-like order and icosahedron-like order, respectively [54]. Thus, it is possible that the soft and hard domains in the HAADF-STEM images in figures 6(a)–(d) have different density and local symmetries.

The structural heterogeneity was further investigated using the 3DAP experiment. Figure 7 presents the elemental maps of the as-quenched Cu-based MG (a slightly crystallized sample was also investigated for comparison, as indicated in figure S8), from which no second nanocrystalline phase precipitated or an apparent phase separation can be detected within the detected resolution of 3DAP. Nevertheless, an obvious structural inhomogeneity is observed from the 1D concentration depth profiles of the Cu, Zr, Al, and Y elements obtained from the selected volume ($5 \times 5 \times 120$ nm^3) marked in the map of all elements in figure 7(a). From figure 7(b), region A has lower average Cu concentration and larger average Zr concentration than region B. Moreover, each peak of the Cu profile curve corresponds well to a valley of the Zr profile curve, as seen from the examples marked by magenta arrows in figure 7(b). This clearly indicates the well-correlated periodic fluctuations of the Zr/Cu element distribution in the $Cu_{46}Zr_{42}Al_7Y_5$ MG. The average wavelength of incipient concentration waves can be determined to be ~5–6 nm for Zr and Cu. This directly results in density fluctuations with Cu-rich (Zr-poor) and Cu-poor (Zr-rich) domains at several nanometers scale. In contrast, Al and Y show random fluctuations, having no apparent correlation with other elements. Thus, the dark and bright domains observed in the HAADF-STEM may be mainly determined by the composition fluctuations of Cu and Zr. However, the contributions from variations of density and cluster symmetry cannot be ruled out. Besides, figures 7(c) and (d) show the statistical binomial frequency distribution analysis of the experimental results, indicating a relatively good match between the fitting binomial curves and

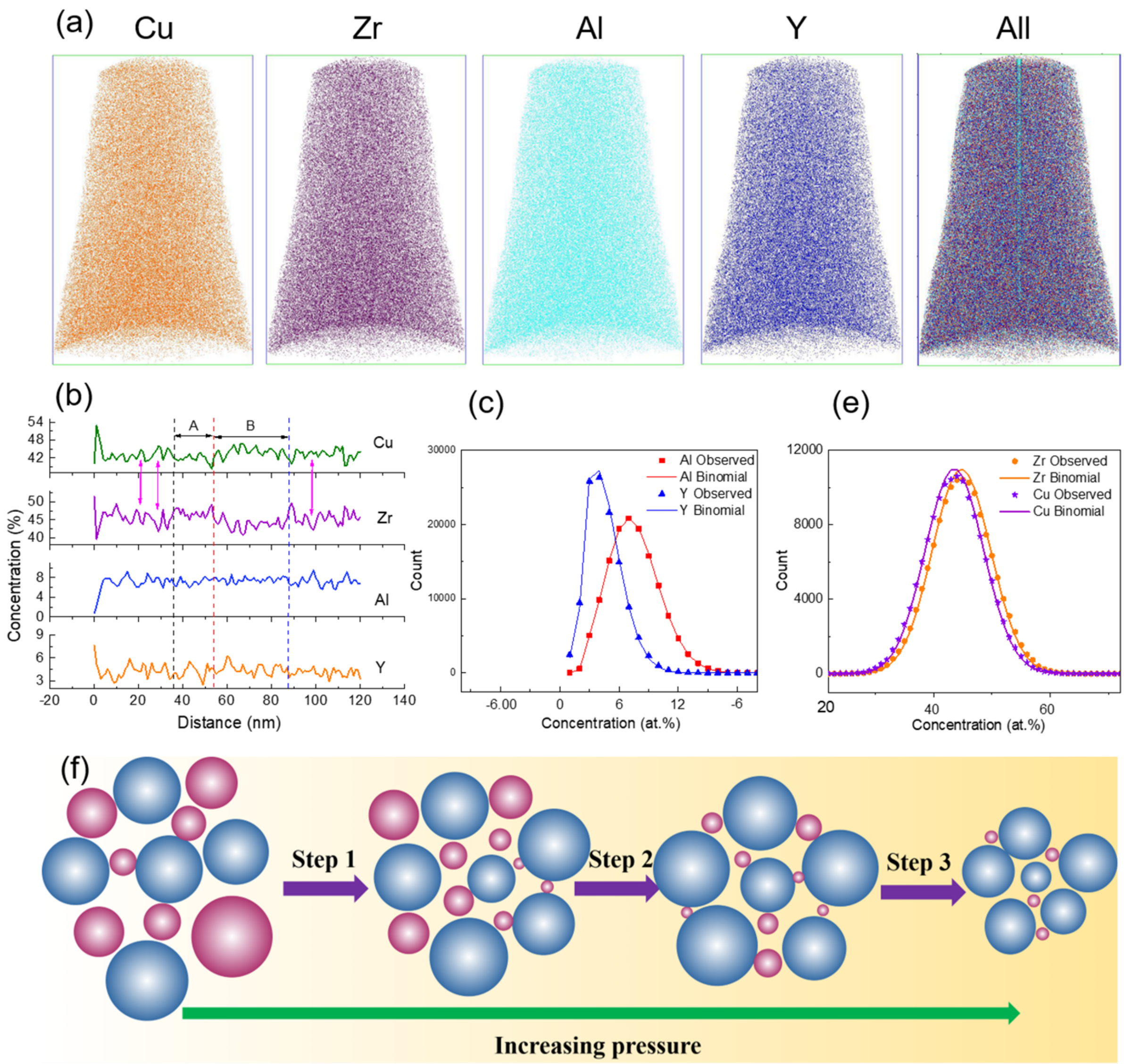

Figure 7. (a) The 3DAP maps of Cu, Zr, Al, Y, and all the elements. (b) One-dimensional concentration profiles from the selected regime ($5 \times 5 \times 120$ nm^3) marked in the all-element map in (a). (c) and (d) Frequency distribution of the elements obtained from experimental data and binomial simulation. (e) Schematic diagram of reorganization of the local network composed of solid-like (blue balls) and liquid-like (purple balls) domains under high pressure.

the experimental curves. The reduced χ^2 parameter indicating the degree of heterogeneity of the elemental distribution can be determined (from $\sum(N_{\mathrm{ob}} - N_{\mathrm{ep}})^2/N_{\mathrm{ep}}$, where N_{ob} is the number of bins observed in the experimental data at a certain elemental concentration, and N_{ep} is the number of bins expected for a homogeneous alloy with random distributions) to be 25.0, 17.0, 2.5, and 47.2 for Cu, Zr, Al, and Y, respectively. This may indicate the most homogeneous distribution of the Al element.

It has been generally accepted that solute-centered clusters can serve as the building blocks for MGs, which construct different types of of MRO by different packing schemes of clusters [3–6]. Especially in the Cu–Zr systems, simulations reveal that a significant fraction of icosahedral clusters exists and tends to form an interpenetrating stringlike backbone network, and the non-interpenetrating connections further promote the connectivity of icosahedral networks, affecting significantly the dynamic heterogeneity and glass formation [56–58]. Note that 53% of the atoms were reported from simulation to be involved in icosahedral clusters in the $Cu_{64}Zr_{36}$ MG [57]; thus, it is possible that a similarly high fraction of atoms participates in the icosahedral-like clusters in the $Cu_{46}Zr_{42}Al_7Y_5$ MG [57], forming stringlike or ringlike networks of these clusters [56, 57]. Accordingly, we will mainly illustrate the steplike polyamorphic transitions from the unique network connections among clusters, which correlate well with the Y addition. First, the Y addition enhances the fraction of the clusters with icosahedral-like symmetry because these clusters are mechanically more stable, easier to aggregate forming backbone, and more long-lived than others [56].

These arguments are supported by the experimental observations of the reduced liquid temperature from 1163 K in $Cu_{46}Zr_{47}Al_7$ to 1113 K in $Cu_{46}Zr_{42}Al_7Y_5$ and the improved glass-forming ability significantly after 5 at.% Y addition [59]. Second, the Y atoms may increase the local chemical heterogeneity considerably because the Y–Zr pair has positive enthalpy mixing ($+35$ kJ mol^{-1}), which is strikingly different from other pairs having large negative enthalpy of mixing: Zr–Cu (-142 kJ mol^{-1}), Cu–Y (-148 kJ mol^{-1}), Zr–Al (-169 kJ mol^{-1}), and Y–Al (-181 kJ mol^{-1}). This results in distinct density and chemical fluctuations on the subnanometer/nanometer scale, as observed experimentally (figures 6 and 7). We argue that chemical heterogeneity, including Cu-rich and Zr-rich dual-glass nanoscale domains, is crucial for the steplike polyamorphism, and that this novel polyamorphism is not observed in the Zr-, Ti-, and Ce-based MGs (having conventional local structural heterogeneity) due to the absence of such kind of chemical heterogeneity.

A cluster-construction model of the present alloy is thus proposed as follows. Many of the Zr-rich clusters (forming the solid-like domain) may have icosahedral-like symmetry and higher density, connecting to form the backbone network [56, 57]. These regions (Cu-rich clusters) with lower density form liquid-like structures surrounding the backbone network. Importantly, the Zr-rich domains and the Cu-rich domains (several nanometers in size) are bridged with each other and form an interconnected network. This unique network structure is consistent with the experimental observations in figures 6(a)–(d) and 7(b). To illustrate the unordinary polyamorphic transition, we focus on the reorganization of a local ring network under compression, as illustrated schematically in figure 7(e). Each ring is composed of a central Zr-rich domain and several (m on average in the as-quenched state) neighboring Zr-rich domains (with typical size as that of the bright domains in figures 6(a)–(d)), which are connected mainly through the Cu-rich domains. This kind of local ring acts as the structural unit on the MRO length scale responding to the external pressure. Under initial compression, these local rings collapse mainly through densification of the liquid-like (Cu-rich) domains (step 1 in figure 7(e)). Under compression, more and more liquid-like domains transform into solid-like domains. Below 8.1 GPa, the local cluster network transforms into a new configuration with an increased average number ($m + 1$) of the solid-like domains in the local ring. Further compression (8.1–14.1 GPa) mainly distorts the domains and rearranges their connections while keeping the density slightly changed due to the hard compression of the Zr–Zr bond length (the inset of figure 4(b)). Above ~14.1 GPa, the MG evolves into a high-density state with the lowest degree of chemical fluctuation (in accord with the simulation), the compression of which is dominated mainly by the solid-like domains (step 3 in figure 7(e)) and takes place more homogeneously than that below 14.1 GPa.

Therefore, the compression plateau is associated with the distortion of and interplay between the Cu-rich and Zr-rich domains in the intermediate state with an increased average number ($m + 1$) of solid-like domains in each local ring (step 2 in figure 7(e)). This transformation behavior is like the compression plateau of the network glass GeO_2 [60, 61]. It was found that the plateau of the FSDP position between 22.6 and 37.9 GPa was related to the formation and stability of sixfold-coordinated structural motifs [62]. The pressure independence of the FSDF between 72.5 and 91.7 GPa arose from the gradual transformation of the sixfold-coordinated structural motifs into stable motifs with higher Ge-O CN [63]. The similar compression behavior between the $Cu_{46}Zr_{42}Al_7Y_5$ MG and GeO_2 implies that they may have some common connection features of their structural motifs. In addition, the different compression behaviors between $Cu_{46}Zr_{42}Al_7Y_5$ and many other MGs indicate the significant impact of the details of structural heterogeneity on the evolution of atomic configuration under compression [19–40, 50]. Finally, we argue that the ultrahigh bulk modulus (directly related to the compression plateau under high pressure) in the intermediate state of $Cu_{46}Zr_{42}Al_7Y_5$ is rooted in the reorganization of the supra-nanometer-sized dual-glass network structures at MRO and the lowest coefficient of compressibility of the Zr–Zr bond length (from simulation) at short-range order. At present, the detailed mechanism of this intriguing behavior requires further study in the future.

In summary, novel steplike polyamorphic transitions are observed in a Cu-based nanostructured MG. We have excluded the contributions from the nanocrystalline phase or some special crystal-like clusters and verified the significant role of the concentration waves of Cu/Zr and the corresponding interconnected network composed of Cu-rich and Zr-rich domains at the nanoscale. At short-range-order length scale, the heterogeneous evolution of the bond lengths of different atomic pairs (especially the Zr–Zr bonds) makes a significant impact on the evolution of the Cu-rich and Zr-rich domains and contributes to the polyamorphism. The present polyamorphic transitions unveil a hidden intermediate state with an unusually high modulus, which opens a new avenue toward advanced MGs with super-mechanical performances by tailoring topological/chemical heterogeneity at nanoscale and supra-nanometer structure engineering. Since chemical heterogeneity, local composition fluctuation, and nanoscale phase separation are facile to create in MGs [64–71], the steplike polyamorphism may exist in other systems.

Acknowledgments

This work was supported by the National Natural Science Foundation of China (Grant Nos. 51971061, 52231005, and 52031016) and the Fundamental Research Funds for the Central Universities (Grant No. 2242020R10003). We would like to thank Shanghai Synchrotron Radiation Facility in Shanghai, China and Synchrotron Radiation Facility in Beijing, China, for use of the synchrotron radiation facilities.

Conflict of interest

The authors declare that they have no conflicts of interest to disclose.

ORCID iD

Qiang Luo https://orcid.org/0000-0001-5682-5536

References

[1] Cheng Y Q and Ma E 2011 Atomic-level structure and structure-property relationship in metallic glasses *Prog. Mater. Sci.* **56** 379–473

[2] Wang W H, Dong C and Shek C H 2004 Bulk metallic glasses *Mater. Sci. Eng.* **44** 45–89

[3] Sheng H W, Luo W K, Alamgir F M, Bai J M and Ma E 2006 Atomic packing and short-to-medium range order in metallic glasses *Nature* **439** 419–25

[4] Miracle D B 2004 A structural model for metallic glasses *Nat. Mater.* **3** 697–702

[5] Ma D, Stoica A D and Wang X L 2009 Power-law scaling and fractal nature of medium-range order in metallic glasses *Nat. Mater.* **8** 30–34

[6] Chen D Z, Shi C Y, An Q, Zeng Q, Mao W L, Goddard W A and Greer J R 2015 Fractal atomic-level percolation in metallic glasses *Science* **349** 1306–10

[7] Wang W H 2007 Roles of minor additions in formation and properties of bulk metallic glasses *Prog. Mater. Sci.* **52** 540–96

[8] Yu B, Wang W H and Samwer K 2013 The beta relaxation in metallic glasses: an overview *Mater. Today* **16** 183–91

[9] Wang Q, Liu J J, Ye Y F, Liu T T, Wang S, Liu C T, Lu J and Yang Y 2017 Universal secondary relaxation and unusual brittle-to-ductile transition in metallic glasses *Mater. Today* **20** 293–300

[10] Zhang C Z, Hu L N, Yue Y Z and Mauro J C 2010 Fragile-to-strong transition in metallic glass-forming liquids *J. Chem. Phys.* **133** 014508

[11] Zhou C, Hu L N, Sun Q J, Zheng H, Zhang C Z and Yue Y Z 2015 Structural evolution during fragile-to-strong transition in CuZr(Al) glass-forming liquids *J. Chem. Phys.* **142** 064508

[12] Concustell A, Méar F O, Suriñach S, Baró M D and Greer A L 2009 Structural relaxation and rejuvenation in a metallic glass induced by shot-peening *Phil. Mag. Lett.* **89** 831–40

[13] Liu Y H, Wang G, Wang R J, Zhao D Q, Pan M X and Wang W H 2007 Super plastic bulk metallic glasses at room temperature *Science* **315** 1385–8

[14] Ye J C, Lu J, Liu C T, Wang Q and Yang Y 2010 Atomistic free-volume zones and inelastic deformation of metallic glasses *Nat. Mater.* **9** 619–22

[15] Dmowski W, Yokoyama Y, Chuang A, Ren Y, Umemoto M, Tsuchiya K, Inoue A and Egami T 2010 Structural rejuvenation in a bulk metallic glass induced by severe plastic deformation *Acta Mater.* **58** 429–38

[16] Pan J, Wang Y X, Guo Q, Zhang D, Greer A L and Li Y 2018 Extreme rejuvenation and softening in a bulk metallic glass *Nat. Commun.* **9** 560

[17] Ketov S V *et al* 2015 Rejuvenation of metallic glasses by non-affine thermal strain *Nature* **524** 200–3

[18] Xu W, Sandor M T, Yu Y, Ke H-B, Zhang H-P, Li M-Z, Wang W-H, Liu L and Wu Y 2015 Evidence of liquid-liquid transition in glass-forming $La_{50}Al_{35}Ni_{15}$ melt above liquidus temperature *Nat. Commun.* **6** 7696

[19] Zhou C, Hu L N, Sun Q J, Qin J, Bian X F and Yue Y Z 2013 Indication of liquid-liquid phase transition in CuZr-based melts *Appl. Phys. Lett.* **103** 171904

[20] Wei S, Yang F, Bednarcik J, Kaban I, Shuleshova O, Meyer A and Busch R 2013 Liquid-liquid transition in a strong bulk metallic glass-forming liquid *Nat. Commun.* **4** 2083

[21] Sheng H W, Liu H Z, Cheng Y Q, Wen J, Lee P L, Luo W K, Shastri S D and Ma E 2007 Polyamorphism in a metallic glass *Nature* **6** 192–7

[22] Belhadi L, Decremps F, Pascarelli S, Cormier L, Le Godec Y, Gorsse S, Baudelet F, Marini C and Garbarino G 2013 Polyamorphism in cerium based bulk metallic glasses: electronic and structural properties under pressure and temperature by x-ray absorption techniques *Appl. Phys. Lett.* **103** 111905

[23] Zeng Q, Ding Y, Mao W L, Yang W, Sinogeikin S V, Shu J, Mao H-K and Jiang J Z 2010 Origin of pressure-induced polyamorphism in $Ce_{75}Al_{25}$ metallic glass *Phys. Rev. Lett.* **104** 105702

[24] Duarte M, Bruna P, Pineda E, Crespo D, Garbarino G, Verbeni R, Zhao K, Wang W H, Romero A H and Serrano J 2011 Polyamorphic transitions in Ce-based metallic glasses by synchrotron radiation *Phys. Rev.* B **84** 224116

[25] Zeng Q S *et al* 2007 Anomalous compression behavior in lanthanum/cerium-based metallic glass under high pressure *Proc. Natl Acad. Sci. USA* **104** 13 565

[26] Zhao X, Wang C Z, Zheng H J, Tian Z A and Hu L N 2017 The role of liquid–liquid transition in glass formation of CuZr alloys *Phys. Chem. Chem. Phys.* **19** 15962–72

[27] Lan S, Ren Y, Wei X Y, Wang B, Gilbert E P, Shibayama T, Watanabe S, Ohnuma M and Wang X L 2017 Hidden amorphous phase and reentrant supercooled liquid in Pd-Ni-P metallic glasses *Nat. Commun.* **8** 14679

[28] Ge J C *et al* 2019 *In-situ* scattering study of a liquid-liquid phase transition in Fe-B-Nb-Y supercooled liquids and its correlation with glass-forming ability *J. Alloys Compd.* **787** 831–9

[29] Li J J Z, Rhim W K, Kim C P, Samwer K and Johnson W L 2011 Evidence for a liquid–liquid phase transition in metallic fluids observed by electrostatic levitation *Acta Mater.* **59** 2166–71

[30] Küchemann S and Samwer K 2016 Ultrafast heating of metallic glasses reveals disordering of the amorphous structure *Acta Mater.* **104** 119–24

[31] Luo Q, Schwarz B, Swarbrick J C, Bednarčik J, Zhu Y, Tang M, Zheng L, Li R, Shen J and Eckert J 2018 Local-structure change rendered by electronic localization delocalization transition in cerium-based metallic glasses *Phys. Rev.* B **97** 064104

[32] Luo Q *et al* 2015 Hierarchical densification and negative thermal expansion under high pressure in Ce-based metallic glass *Nat. Commun.* **6** 5703–11

[33] Li L, Luo Q, Li R, Zhao H, Chapman K W, Chupas P J, Wang L and Liu H 2017 Polyamorphism in Yb-based metallic glass induced by pressure *Sci. Rep.* **7** 46762

[34] Wang X Y, Wang W K, Zhan Z J, Xu F Y, Zhang N Y, Wang F X, Chen Y, Pang Y T, Zhao L P and Wang J 2007 Compression behaviour and micro-structure evaluation of $Zr_{57}Nb_5Cu_{15.4}Ni_{12.6}Al_{10}$ bulk metallic glass under high pressure *Mater. Lett.* **61** 2170–2

[35] Sheng H W, Ma E, Liu H Z and Wen J 2006 Pressure tunes atomic packing in metallic glass *Appl. Phys. Lett.* **88** 171906

[36] Li G, Xin-Yu Z, Yi-Nan S, Yu-Qing Q, Jing L and Ri-Ping L 2005 Compression behaviour of $Ni_{77}P_{23}$ amorphous alloy up to 30.5 GPa *Chin. Phys. Lett.* **22** 2615

[37] Stemshorn A K and Vohra Y K 2009 Structural stability and compressibility of group IV transition metals-based bulk metallic glasses under high pressure *J. Appl. Phys.* **106** 046101

[38] Li L L, Wang L, Li R, Zhao H, Qu D, Chapman K W, Chupas P J and Liu H 2016 Constant real-space fractal dimensionality and structure evolution in $Ti_{62}Cu_{38}$ metallic glass under high pressure *Phys. Rev.* B **94** 184201

[39] Mattern N, Bednarcik J, Liermann H and Eckert J 2013 Structural behaviour of $Pd_{40}Cu_{30}Ni_{10}P_{20}$ metallic glass under high pressure *Intermetallics* **38** 9–13

[40] Tomizukat A, Iwasakit H, Fukamichi K and Kikegawa T 1984 High-pressure x-ray diffraction study of magnetoelastic properties of Fe-based amorphous alloys *J. Phys. F: Met. Phys.* **14** 1507–14

[41] Lou H B *et al* 2012 Pressure-induced amorphous-to-amorphous configuration change in Ca-Al metallic glasses *Sci. Rep.* **2** 376

[42] Du Q, Liu X-J, Zeng Q, Fan H, Wang H, Wu Y, Chen S-W and Lu Z-P 2019 Polyamorphic transition in a transition metal based metallic glass under high pressure *Phys. Rev.* B **99** 014208

[43] Katayama Y, Mizutani T, Utsumi W, Shimomura O, Yamakata M and Funakoshi K-I 2000 A first-order liquid–liquid phase transition in phosphorus *Nature* **403** 170–3

[44] Sen S, Gaudio S, Aitken B G and Lesher C E 2006 A pressure-induced first-order polyamorphic transition in a chalcogenide glass at ambient temperature *Phys. Rev. Lett.* **97** 025504

[45] Morishita T 2004 High density amorphous form and polyamorphic transformations of silicon *Phys. Rev. Lett.* **93** 055503

[46] Mishima O, Calvert L D and Whalley E 1985 An apparently first-order transition between two amorphous phases of ice induced by pressure *Nature* **314** 76–78

[47] Yavari A R, Moulec A L, Inoue A, Nishiyama N, Lupu N, Matsubara E, Botta W J, Vaughan G, Michiel M D and Kvick Å 2005 Excess free volume in metallic glasses measured by x-ray diffraction *Acta Mater.* **53** 1611

[48] Zeng Q *et al* 2014 Universal fractional noncubic power law for density of metallic glasses *Phys. Rev. Lett.* **112** 185502

[49] Zeng Q *et al* 2016 General 2.5 power law of metallic glasses *Proc. Natl Acad. Sci. USA* **113** 1714–8

[50] Li G, Wang Y Y, Liaw P K, Li Y C and Liu R P 2012 Electronic structure inheritance and pressure-induced polyamorphism in lanthanide-based metallic glasses *Phys. Rev. Lett.* **109** 125501

[51] Giintherodt H J and Beck H 1981 Glass metals: I *Topics in Applied Physics* vol 46 (Berlin: Springer)

[52] Wang Q, Liu C T, Yang Y, Liu J B, Dong Y D and Lu J 2014 The atomic-scale mechanism for the enhanced glass-forming-ability of a Cu-Zr based bulk metallic glass with minor element additions *Sci. Rep.* **4** 4648

[53] Wagner H, Bedorf D, Küchemann S, Schwabe M, Zhang B, Arnold W and Samwer K 2011 Local elastic properties of a metallic glass *Nat. Mater.* **10** 439–42

[54] Zhu F, Hirata A, Liu P, Song S, Tian Y, Han J, Fujita T and Chen M 2017 Correlation between local structure order and spatial heterogeneity in a metallic glass *Phys. Rev. Lett.* **119** 215501

[55] Huang B *et al* 2018 Density fluctuations with fractal order in metallic glasses detected by synchrotron X-raynano-computed tomography *Acta Mater.* **155** 69–79

[56] Li M Z, Wang C Z, Hao S G, Kramer M J and Ho K M 2009 Structural heterogeneity and medium-range order in Zr_xCu_{100-x} metallic glasses *Phys. Rev.* B **80** 184201

[57] Soklaski R, Nussinov Z, Markow Z, Kelton K F and Yang L 2013 Connectivity of the icosahedral network and a dramatically growing static length scale in Cu-Zr binary metallic glasses *Phys. Rev.* B **87** 184203

[58] Hu Y C, Li F X, Li M Z, Bai H Y and Wang W H 2015 Five-fold symmetry as indicator of dynamic arrest in metallic glass-forming liquids *Nat. Commun.* **6** 8310

[59] Xu D, Duan G and Johnson W L 2004 Unusual glass-forming ability of bulk amorphous alloys based on ordinary metal copper *Phys. Rev. Lett.* **92** 245504

[60] Mei Q, Sinogeikin S, Shen G, Amin S, Benmore C J and Ding K 2010 High-pressure x-ray diffraction measurements on vitreous GeO_2 under hydrostatic conditions *Phys. Rev.* B **81** 174113

[61] Hong X, Shen G, Prakapenka V B, Newville M, Rivers M L and Sutton S R 2007 Intermediate states of GeO_2 glass under pressures up to 35 GPa *Phys. Rev.* B **75** 104201

[62] Hong X, Ehm L and Duffy T S 2014 Polyhedral units and network connectivity in GeO_2 glass at high pressure: an x-ray total scattering investigation *Appl. Phys. Lett.* **105** 081904

[63] Kono Y, Kenney-Benson C, Ikuta D, Shibazaki Y, Wang Y and Shen G 2016 Ultrahigh-pressure polyamorphism in GeO_2 glass with coordination number > 6 *Proc. Natl Acad. Sci. USA* **113** 3436–41

[64] Park E S and Kim D H 2006 Phase separation and enhancement of plasticity in Cu-Zr-Al-Y bulk metallic glasses *Acta Mater.* **54** 2597–604

[65] Sohn S W, Yook W, Kim W T and Kim D H 2012 Phase separation in bulk-type Gd-Zr-Al-Ni metallic glass *Intermetallics* **23** 57–62

[66] Witte R, Feng T, Fang J X, Fischer A, Ghafari M, Kruk R, Brand R A, Wang D, Hahn H and Gleiter H 2013 Evidence for enhanced ferromagnetism in an iron-based nanoglass *Appl. Phys. Lett.* **103** 073106

[67] Wang J Q, Chen N, Liu P, Wang Z, Louzguine-Luzgin D V, Chen M W and Perepezko J H 2014 The ultrastable kinetic behavior of an Au-based nanoglass *Acta Mater.* **79** 30–36

[68] Yang W, Li J, Li H, Liu H, Mo J, Lan S, Li M, Wang X L, Eckert J and Huo J 2022 Inheritance factor on the physical properties in metallic glasses *Mater. Futures* **1** 035601

[69] Yuan C C, Lv Z W, Pang C M, Li X, Liu R, Yang C, Ma J, Ke H B, Wang W H and Shen B L 2021 Ultrasonic-assisted plastic flow in a Zr-based metallic glass *Sci. China Mater.* **64** 448–59

[70] Qiao J C, Wang Q, Pelletier J M, Kato H, Casalini R, Crespo D, Pineda E, Yao Y and Yang Y 2019 Structural heterogeneities and mechanical behavior of amorphous alloys *Prog. Mater. Sci.* **104** 250–329

[71] Zhang J Y, Zhou Z Q, Zhang Z B, Park M H, Yu Q, Li Z, Ma J, Wang A D, Huang H G and Song M 2022 Recent development of chemically complex metallic glasses: from accelerated compositional design, additive manufacturing to novel applications *Mater. Futures* **1** 012001